

Article

Frequency Regulation of Power Systems with Self-Triggered Control under the Consideration of Communication Costs

Zhiqin Zhu ^{1,2}, Jian Sun ^{2,*}, Guanqiu Qi ³ , Yi Chai ⁴ and Yinong Chen ³

¹ College of Automation, Chongqing University of Posts and Telecommunications, Chongqing 400065, China; zhuzq@cqupt.edu.cn

² College of Electronic and Information Engineering, Southwest University, Chongqing 400715, China

³ School of Computing, Informatics, and Decision Systems Engineering, Arizona State University, Tempe, AZ 85287, USA; guanqiuq@asu.edu (G.Q.); yinong@asu.edu (Y.C.)

⁴ State Key Laboratory of Power Transmission Equipment and System Security and New Technology, Chongqing University, Chongqing 400044, China; chaiyi@cqu.edu.cn

* Correspondence: cq_jsun@163.com

Academic Editor: Johannes Kiefer

Received: 9 April 2017; Accepted: 30 June 2017; Published: 4 July 2017

Abstract: In control systems of power grids, conveying observations to controllers and obtaining control outputs depend greatly on communication and computation resources. Particularly for large-scale systems, the costs of computation and communication (cyber costs) should not be neglected. This paper proposes a self-triggered frequency control system for a power grid to reduce communication costs. An equation for obtaining the triggering time is derived, and an approximation method is proposed to reduce the computation cost of triggering time. In addition, the communication cost of frequency triggering is measured quantitatively and proportionally. The defined cost function considers both physical cost (electricity transmission cost) and communication cost (control signal transmission cost). The upper bound of cost is estimated. According to the estimated upper bound of cost, parameters of the controller are investigated by using the proposed optimization algorithm to guarantee the high performance of the system. Finally, the proposed self-triggered power system is simulated to verify its efficiency and effectiveness.

Keywords: frequency regulation; self-triggered control; input to state stable; communication cost

1. Introduction

Control systems have been widely used in power grids, and large-scale control systems continually increase the proportion of usage. Due to limited computation and communication resources, the traditional electric power network seriously affects the performance of large-scale control systems. The public shared networks for control signal communication, such as the Internet, have more powerful computation and communication resources which are used to increase the efficiency of current large-scale control systems. The scheduling of computation capacity and communication bandwidth is the key to efficiently utilizing public shared networks. Event-triggered control (ETC) systems are used to reduce the costs of computation and energy resources when the electricity network is in a steady state. They avoid the limited bandwidth of the communication network occupied by redundant sampled and fused signals [1–6]. The self-triggered control (STC) method [7,8] as one of the control methods can effectively reduce communication costs and power costs of sensor monitoring in the control system. An STC method is applicable to solve the optimization of scheduling computation and communication resources, especially in networked control systems (NCSs). The control task is triggered when STC is at the pre-computed updating time.

Since more and more systems have become increasingly networked, wireless, and spatially distributed, event-based systems are proposed to adopt a model of calls for resources only if necessary, and to utilize communication bandwidth, computation capability, and energy budget efficiently [9–12]. The proposed control-based model allowed each control task to trigger itself to achieve the optimization of computing resources and control performance. The execution time of next instance was scheduled by the executing instance. As a function of the utilization factor and control performance, the next instance execution point was dynamically obtained in time [13–17]. The dynamic selection of an appropriate threshold was investigated for basic send-on-delta (SoD) sampling strategies. The error reduction principle was formulated and proved to reduce the signal tracking-error in an available transmission rate [18,19]. A new event-based control strategy was proposed and applied to differential wheeled robots. Compared with the classical discrete-time strategy, the proposed event-based control strategy not only reached the same accuracy, but also obtained a higher efficiency in communication resource usage [20–23].

In power system frequency regulation research, Shashi Kant Pandey [24] used linear matrix inequalities (LMI) with parameters tuned by particle swarm optimization (PSO). Praghmesh Bhatt [25] analyzed the dynamic participation of doubly-fed induction generators and coordinated control for frequency regulation of an interconnected two-area power system in a restructured competitive electricity market. Soumya R. Mohanty [26] presented a study on frequency regulation in an isolated hybrid distributed generation (DG) system with the robust H-infinite loop shaping controller. Although much frequency regulation research has been done in order to achieve better physical performances, cyber costs also need to be taken into account. Considering both physical performance and the cyber cost of power system, event-driven schemes are usually used. Dai [27] proposed a methodology for real-time prediction that required event-driven load shedding (ELS) against severe contingency events. Jun [28] presented a novel emergency damping control (EDC) to suppress inter-area oscillations occurring as anticipated low-probability cases in power system operations. The proposed EDC combined an event-driven scheme and a response-based control strategy. Yan [29] elaborated a new approach based on parallel-differential evolution (P-DE) to efficiently and globally optimize ELS against voltage collapse.

However, continuously monitoring plants using event-driven schemes takes many cyber resources. In contrast with the EDC approach, STC does not generally require dedicated hardware to continuously monitor the plant state and check the defined stability conditions [30–33]. Therefore, STC can be considered in power grid frequency regulation to reduce communication costs and make the utilization of communication resources more efficient.

In this paper, we propose a novel self-triggered control scheme employed in a frequency-controlled power grid. A power grid consists of many subsystems that interact with each other through communication networks and power flow. The proposed self-triggered controller calculates the triggering period with each state point to ensure the system's exponential stability, input-to-state stability, and low communication cost. In the proposed model, the triggering interval is a function of system state and triggering rate is proportional to communication cost. This paper has three main contributions as follows:

- A self-triggered control scheme is applied to the frequency regulation of the power grid;
- An online optimization method is used to extend the triggering period for reducing communication cost; and
- Communication cost and parameters of control system for power grid are estimated and optimized, so that the cost of control system can be guaranteed under a required level.

This paper is organized as follows. Section 2 introduces the model of the power system and the basic concept used in this paper. Section 3 presents the proposed self-triggered control scheme in which the exponential stability theory with varying sampling rate, control performance synthesis algorithm for the control system under the consideration of communication, physical cost and online

optimization for searching the maximal triggering period are elaborated. A simulation of frequency regulation with a self-triggered control scheme is illustrated in Section 4. Conclusions are given in Section 5.

2. System Model of Power Grid

2.1. Dynamic Model of Power Grid

The electric power network consists of n interconnected power subsystems as shown in Figure 1. It assumes that all power subsystems are same. Each power subsystem consists of a distributed energy source and load, including gas turbine generators, wind power generations and battery arrays [34,35] in the system. These power generating machines supply electric power to meet the demands. Gas turbine, wind power, and battery power output are controllable.

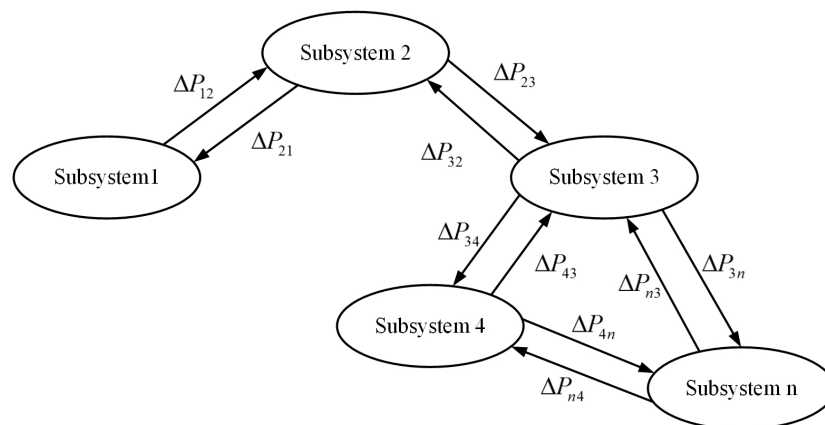


Figure 1. Power grid structure.

Mass loads are considered in the dynamic model of the power grid. Battery electric storage systems and wind power systems, which are connected to the power net by power electronic interface, are controllable. In mathematics, the frequency control method is equivalent to the tie-line bias control (TBC) method as a frequency control in electrical power systems in consideration of tie-line frequency [36–39]. For each subsystem, the block diagram is shown in Figure 2. The meaning of each parameter in the block diagram is given as follows.

- K_i and B_i are TBC gain and frequency bias, respectively.
- T_{gi} and T_{di} are the governor and gas turbine constant, respectively.
- M_i and D are the inertia and damping constant, respectively.
- R_{gi} and T_{ij} are the regulation and synchronizing constant, respectively.
- Δx_{gi} is a governor input of a gas turbine generator.

There are six power notations as follows:

- ΔP_{gi} is an output of the gas turbine generator.
- ΔP_{Wi} is an output of wind power generation.
- ΔP_{Li} is the load fluctuation except controllable load.
- ΔP_{Bi} is an output of the battery electric storage system.
- ΔP_{ji} and ΔP_{ij} is the tie-line power low deviation.
- $\Delta P_{ij} - \Delta P_{ji}$ is the output power of area i , which is delivered to area j .
- ΔP_i in Equation (1) shows the electric power generation of subsystem i and the supply error margin of power consumption.

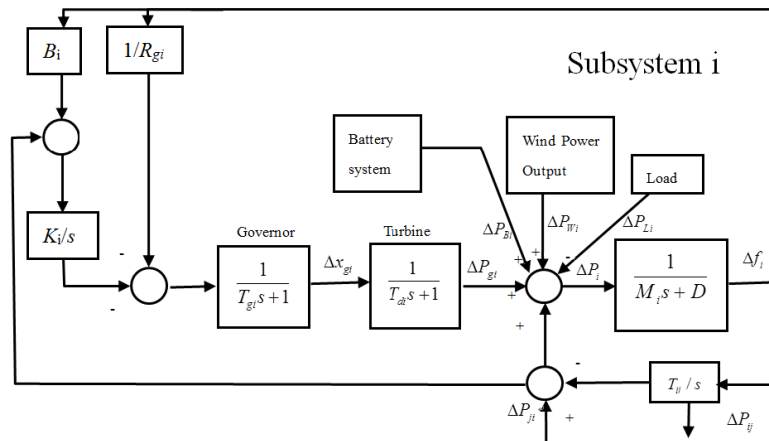


Figure 2. Subsystem structure.

Frequency deviation Δf_i can be calculated by the supply error margin shown in the block diagram. The power ΔP_i for subsystem *i* is:

$$\Delta P_i = \Delta P_{gi} + \Delta P_{Wi} + \Delta P_{Bi} - \Delta P_{Li} + \Delta P_{ij} - \Delta P_{ji} \tag{1}$$

In a mathematical form, for subsystem *i*, if the set of neighbored subsystem is denoted as D_i , the dynamics of each subsystem can be described by using continuous time-state equation:

$$\dot{x}_i = A_i x_i + B_i u_i + \sum_{j \in D_i} A_{ji} x_j + E_i w_i \tag{2}$$

$$A_i = \begin{pmatrix} 0 & -\sum_{j \in D_i} T_{ji} & 0 & 0 & 0 \\ 1/M_i & -D_i/M_i & 1/M_i & 0 & 0 \\ 0 & 0 & -1/T_{di} & 1/T_{di} & 0 \\ 0 & -1/(T_{gi}R_{gi}) & 0 & 1/T_{gi} & K_i/T_{gi} \\ 1 & -B_i & 0 & 0 & 0 \end{pmatrix},$$

$$B_i = \begin{pmatrix} 0 & 0 \\ 1/M_i & 1/M_i \\ 0 & 0 \\ 0 & 0 \\ 0 & 0 \end{pmatrix},$$

$$A_{ji} = \begin{pmatrix} 0 & 0 & 0 & 0 & 0 \\ \frac{T_{ij}}{M_i \sum_{h \in D_i} T_{ih}} & 0 & 0 & 0 & 0 \\ 0 & 0 & 0 & 0 & 0 \\ 0 & 0 & 0 & 0 & 0 \\ 0 & 0 & 0 & 0 & 0 \end{pmatrix}, j \in D_i.$$

where $x = (\Delta P_{outi}, \Delta f_i, \Delta P_{gi}, \Delta x_{gi} U_{AR_i})^T$, and ΔP_{outi} , Δf_i , ΔP_{gi} , Δx_{gi} , and U_{AR_i} are output power deviation, frequency deviation, gas generator output power deviation, governor input of gas turbine generator, and regional demand for subsystem i , respectively. w_i is disturbance of the dynamic system, which is bounded. The power output of subsystem i is $\Delta P_{outi} = \sum_{j \in D_i} \Delta P_{ij}$. The tie-line power flow deviation of i is expressed as $\Delta \sum_{j \in D_i} P_{ji} = \sum_{j \in D_i} T_{ij}(\Delta f_j B_i \Delta f_i)$, when the adjoining area is j . The regional demand is defined by $U_{AR_i} = \int AR_i dt$, where $AR_i = \Delta \sum_{j \in D_i} P_{ji}$.

For subsystem i , we assume the L-2 norm of w_i is bounded, and $\|w_i\|^2 \leq \eta$. The control input u_i for subsystem i is:

$$u_i = -K_i x_i - \sum_{j \in D_i} L_{ji} x_j, \tag{3}$$

where K is the local state feedback gain for control law of Equation (3), $-K_i x_i$ is the local feedback component and $-\sum_{j \in D_i} L_{ji} x_j$ is the control compensation for the neighbors.

2.2. The Self-Triggered Controller

Compared with the distributed control scheme, the advantage of the centralized control scheme in STC is that it reduces the conservativeness of control system, and further decreases the communication cost [40,41]. In order to present the self-triggered control scheme, the power system is formulated as a linear dynamic system in a form of:

$$\dot{x} = Ax + Bu + EW \tag{4}$$

where $x = (x_i)_{n \times 1}$, $1 \leq i \leq n$ and $i \in N^+$; $A = (A_{ij})_{n \times n}$, $A_{ii} = A_i$, $1 \leq i, j \leq n$ and $i, j \in N^+$, if no connection exists between subsystem i and j , $A_{ij} = 0$; $B = \text{diag}(B_i)_{n \times 1}$ and $E = \text{diag}(E_i)_{n \times 1}$, $1 \leq i \leq n$ and $i, j \in N^+$; the control input $u = (u_i)_{n \times 1} = (-L_{ij})_{n \times n}$, $x = -Kx$, $L_{ii} = K_i$, $1 \leq i, j \leq n$ and $i, j \in N^+$, and $L_{ij} = 0$, if there is no connection on subsystems i and j ; the disturbance is $W = (w_i)_{n \times 1}$, $1 \leq i, j \leq n$ and $i, j \in N^+$. The control objective is to drive state x to origin zero by the linear controller.

In a self-triggered control scheme [42], the local state $x_i(t)$ can be acquired by observers (sensors). However, the information remains within the i th subsystems and is not shared within the system controller unless a pre-calculated triggering time is up, a self-triggered state is reached and a message is sent via data communication links. Thus, the control signal from controller remains constant and may change only after a self-triggered message is received. Self-triggered control promises the reduction of communication cost without sacrificing control performance. For a self-event triggered controller, the dynamic of power system in k th triggering is:

$$\dot{x}(t) = Ax(t) + Bu(t_k) + EW(t), t_k \leq t < t_{k+1} \tag{5}$$

and the control output $u(t_k)$ is:

$$u(t_k) = (-L_{ij})_{n \times n} x(t_k), 1 < i, j < n \text{ and } i, j \in N^+ \tag{6}$$

As shown in Figure 3, for a self-triggered control scheme, the controller obtains system state x_1, x_2, x_3 from sensors or observers of each subsystem, when the time for triggering t_k is up. Then, the next triggering time t_{k+1} is calculated by using the previous system state $x(t_k)$. Meanwhile, the controller calculates the new control output $u(t_k)$ with the obtained new system state. The new control output $u_1(t) = u_1(t_k), u_2(t) = u_2(t_k), u_3(t) = u_3(t_k)$, where $t_k \leq t < t_{k+1}$ is then applied to its corresponding subsystems. Above all, the procedure of self-triggered control is:

1. First, obtain the system state of each subsystem, when the time for triggering is up;
2. Second, calculate the time for the next triggering;

- Finally, apply the new control output, which is calculated by using the system state obtained in step 1.

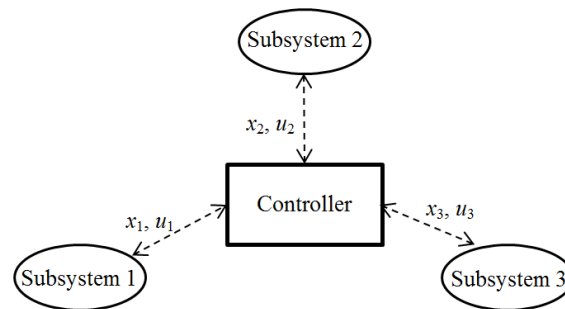


Figure 3. Self-triggered control scheme.

2.3. Exponential Stability and Cost Function

Before elaborating the control scheme for power grid, the exponential stability and cost function are introduced. Exponential stability [43,44] is a kind of asymptotic stability. According to the exponential stability, the state converges to zero with an exponential rate, and $x(t) = x(0)e^{-t}$. If a Lyapunov function satisfies $\kappa_1|x| \leq V(x) \leq \kappa_2|x|$, we have Proposition 1.

Proposition 1 [45]. Let $V : R^n \rightarrow R^+$ be a quadratic Lyapunov candidate function satisfying $V(x) = x^T Px, \forall x \in R^n$, with $P = P^T > 0$. If the condition:

$$\dot{V}(x) + 2\beta V(x) \leq 0 \tag{7}$$

is satisfied for all trajectories of (4), for a given scalar $\beta > 0$, the system origin is globally β -stable (i.e., there exists a scalar β and α , such that the trajectories satisfy $\|x(t)\| \leq \alpha e^{-\beta t} \|x_0\|$ for any initial condition x_0). Proposition 1 addresses the relationship between the time derivation of Lyapunov function $V(x)$ and the $V(x)$ under the restriction of exponential stability.

As both physical cost and cyber cost are considered, the cost of system consists of two parts. The first part, the physical state cost expressed by the following equation, is a general form that is widely used in optimal control theory [46].

$$p(t) = x(t)^T Q x(t) = \|x(t)\|_Q^2$$

where Q is the weight matrix for state cost. The communication cost as the second part is essentially related to the triggering rate. High triggering rate means high communication bandwidth cost in data transmission within a time unit. Therefore, the communication cost is proportional to the sampling rate.

Definition 1. At the k th triggering period, the communication cost is defined as:

$$c(t) = \frac{q}{\tau(k)}.$$

where q is the weight of communication cost, and $\tau(k)$ is the sampling interval between number k sampling and the number $k + 1$ sampling.

Integrating physical state cost with communication cost, the cost function is shown as:

$$\begin{aligned} J &= \int_0^{T_f} [q(t) + c(t)] dt \\ &= \int_0^{T_f} [\|x(t)\|_Q^2 + \frac{q}{\tau(k)}] dt \end{aligned} \tag{8}$$

where T_f is the terminal time. When $t = T_f$, the system state converges to a small value that is close to zero. Moreover, when $t = T_f$, the Lyapunov function value is V_T , which is much smaller than the initial Lyapunov function value V_0 . c is the number of control actions, which have $T_f = \sum_{i=0}^n \tau(i)$. This model considers two parts. The first is a function $\sigma(x(t_k)) = t_{k+1} - t_k$ for calculating self-triggered time, which is adaptive to state $x(t_k)$, to reduce costs in communication; the second is the determination of control gain $K = (-L_{ij})_{n \times n}$. Hence, the cost of system J is guaranteed under a specified upper bound. The following assumptions are made to calculate the upper bound.

Assumption 1. For a given Lyapunov function $V(x) = x^T P x$, ϵ and initial state x_0 , the system is exponentially stable. The terminal time of control process is T_f defined by $dV(x(T_f))/dt = \nu$, where ν is a small number. The Lyapunov function is $V(x(T_f)) = V_T$, and its initial value is $V(x(0)) = V_0$, which has $V_T < V_0$.

Assumption 1 is applied to make the value of Lyapunov function close to zero at terminal time T_f , so that the terminal time T_f for cost function can be determined. It should be noted that the variation of the Lyapunov function converges to zero, when the system converges to a stable state. Therefore, ν should be a small number.

3. The Self-Triggered Controller Design

3.1. Function σ for Self Triggering

The communication cost of self-triggered control depends on the triggering rate, which is directly related to the triggering time in self-triggered control. The system calculates the next triggering time and updating control output when the triggering time is up. The function σ for self-triggering is a crucial function. For obtaining the function σ , some important results about exponential stability and input-to-state stability under self-triggered control are introduced. To investigate the relationship between the maximal triggering interval function σ and system performance, exponential stability and input-to-state stability from disturbance W to system state x , Theorem 1 is proposed.

Theorem 1. For the dynamic system (5), given scalars $\beta > 0, \gamma > 0$, if there exists an $n \times n$ matrix $P = P^T$, a positive scalar γ and a bounded function $\sigma(x) : R^n \rightarrow R_+$ are for all $x \in R^{4n}$ and $\tau \in [0, \sigma(x)]$:

$$x^T \Phi_{P,\beta}(\tau)x \leq \psi(\tau) \tag{9}$$

where ψ is,

$$\psi = \begin{cases} 0 & \tau \in R_1 \cap R_2 \\ (\gamma/2 - (2\beta + 1)(e^{\alpha\tau} - 1)r\epsilon)n\eta & \tau \in R_1/R_2 \\ (\gamma/2 - r\epsilon e^{\alpha\tau})n\eta & \tau \in R_2/R_1 \\ (\gamma - r\epsilon e^{\alpha\tau}(2\beta + 1)(e^{\alpha\tau} - 1)r\epsilon)n\eta & \tau \in R^+/R_1/R_2 \end{cases}$$

with $R_1 = \{\tau | \gamma/2 - r\epsilon e^{\alpha\tau} > 0\}$, $R_2 = \{\tau | \gamma/2 - (2\beta + 1)(e^{\alpha\tau} - 1)r > 0\}$, $\alpha = \lambda_{max}(A^T + A)$, $\epsilon = \lambda_{max}(P)$, $r = \lambda_{max}(E^T E)$, where,

$$\Phi_{P,\beta}(\tau) = \begin{pmatrix} \Lambda(\tau) \\ I \end{pmatrix}^T \begin{pmatrix} A^T P + PA + 2\beta P & -PBK \\ -K^T B^T P & 0 \end{pmatrix} \begin{pmatrix} \Lambda(\tau) \\ I \end{pmatrix} \tag{10}$$

and,

$$\Lambda(\tau) = I + \int_0^\tau e^{sA} ds (A - BK), \tag{11}$$

then the origin system (2) is global β -stable and input-to-state stability from W to x for any triggering interval $\sigma(x) : R_+ \times R^n \rightarrow R_+$ defines the triggering interval sequence by the law $t_{k+1} = t_k + \sigma(x(t_k))$, $k \in N$. $\|x\|^2 \leq n(\gamma + \vartheta)\eta / (\epsilon\beta)$ under a given zero initial state $x(t_k) = 0$.

Proof. See Appendix A. \square

The key of Theorem 1 is that the function σ must satisfy the inequality (9). However directly solving inequality (9) for obtaining σ is difficult. Approaches, such as in [30,47], are employed to cut the triggering interval (sampling interval) and state space into several sections. Numerical methods, such as the linear matrix inequality (LMI) toolbox, offer a possibility to solve σ . The precision of maximal triggering time depends on the number of sections. Higher precision of maximal triggering time requires more sections. In addition, if the state space dimension is high, the computation cost in the design process dramatically increases. This is not practical in power system control applications with a high state space dimension. Therefore, another algorithm is proposed. The $\sigma(x)$ can be directly computed with a given x on-line by the proposed algorithm. Based on the result of Theorem 1, the following theorem is derived for calculating σ .

Theorem 2. For the given parameters in Theorem 1, the dynamic system in Equation (5) has a minimal triggering interval for the global state space $\tau_{min} = \min_{x \in R^{4n}} \sigma(x)$, and a maximal sampling interval $\tau_{max} = \max_{x \in R^{4n}} \sigma(x)$. $\forall \tau \in [0, \sigma(x)]$, $x^T \Phi_{P,\beta}(\tau)x \leq 0$, if the $\sigma(x)$ is:

$$\sigma(x) = \arg_{\tau \in [\tau_{min}, \tau_{max}]} \min \tau, \tag{12}$$

where τ_{min} and τ_{max} are the lower bound and upper bound of self-triggering interval or sampling interval, respectively. Under the constraint of:

$$x^T \Phi_{P,\beta}(\tau)x = \psi(\tau) \tag{13}$$

then the origin system in Equation (2) is global β -stable with input-to-state stability from W to x .

Proof. From Theorem 1, it is known that the left-hand-side and the right-hand side of inequalities (9) are continuous, and $\sigma(x) \in [\tau_{min}, \tau_{max}]$, thus the maximal triggering interval $\sigma(x)$ must be the minimal root of Equation (13).

From Theorem 2, for a given triggering interval $\tau = t_{k+1} - t_k$, the root of Equation (13) for triggering interval $\sigma(x)$ should be the one which is closest to τ_{min} . Equation (13) can be written as a linear combination of $e^{\lambda_i \tau}$ and $e^{(\lambda_i + \lambda_j) \tau}$, where λ_i and λ_j are the eigenvalues of A . If we denote e^τ by z ,

$$\Phi_{P,\beta}(\tau) = \phi_1 + \phi_2 z^{v_1} + \phi_3 z^{v_2} + \dots + \phi_r z^{v_{r-1}} \tag{14}$$

where ϕ_k is the coefficient matrix of z^{v_k} , v_k is λ_i or $\lambda_i + \lambda_j$, $i \leq n, j \leq n$ and $v_i \neq v_j$. However, the computation cost of directly solving the equation $x^T \Phi_{P,\beta}(\tau)x = 0$ is very high, and it is not practical in online processing for power system control. Instead, the approximate root of this equation can be obtained by the two-point Taylor expansion method. The $\Phi_{P,\beta}(\tau)$ can be expanded into two-point Taylor series in m orders at $z_1 = e^{\tau_{min}}$ and $z_2 = e^{\tau_{max}}$. The approximation of $\Phi_{P,\beta}(\tau)$ is:

$$H(z) = \sum_{k=0}^m \{ [a_k(z_1, z_2)(z - z_1) + a_k(z_2, z_1)(z - z_2)] (z - z_1)^k (z - z_2)^k \}, \tag{15}$$

where $z = e^\tau$, and $a_n(z_1, z_2)$ is:

$$a_n(z_1, z_2) = \sum_{k=0}^m \left\{ \frac{(n+k-1)!}{k!(n-k)!} \frac{(-1)^{n+1} n \phi^{(n-k)}(z_2) + (-1)^k k \phi^{(n-k)}(z_1)}{n!(z_1 - z_2)^{n+k+1}} \right\}. \tag{16}$$

and the approximation of the right hand side of Equation (13), denoted $h(z)$, can be obtained similarly as $H(z)$. Above all, for a given state x , we have the following theorem to calculate the $\sigma(x)$. \square

Theorem 3. For the given parameters in Theorem 1, the dynamic system (5), the maximal and minimal triggering intervals τ_{min} , τ_{max} , and the maximal approximation error of $\Phi_{P,\beta}(\tau)$:

$$\varepsilon_1 = \max_{\tau \in [\tau_{min}, \tau_{max}]} \text{eig}[\Phi_{P,\beta}(\tau) - H(z)]$$

The maximal approximation error of $h(z)$ is $\varepsilon_2 = \max_{\tau \in [\tau_{min}, \tau_{max}]} \psi_1(\tau) - h_1(z)$, under $\gamma - r\epsilon e^{\alpha\tau} > 0$, with the approximation expression (15). Then, under the constraint of $\sigma(x) \in [\tau_{min}, \tau_{max}]$, the maximal triggering interval function is chosen by:

$$\sigma(x) = \ln z_c \tag{17}$$

where,

$$z_c = \arg_z \min_{x^T[H(z)+\varepsilon_1 I]x=h_1(z)-\varepsilon_2} |z - z_1| \tag{18}$$

Then, the origin system in Equation (2) is global β -stable with input-to-state stability from W to x .

Proof. See Appendix B. \square

For a given state x , z_c can be easily obtained by solving the polynomial in Equation (18). Thus, under the constraint of $\sigma(x) \in [\tau_{min}, \tau_{max}]$, the maximal triggering interval can be obtained by Theorem 3. If the approximation error ε_1 and ε_2 are very small, the approximation maximal triggering interval obtained by applying Theorem 3 should be very close to the actual maximal triggering interval. It should be noted that τ_{min} can be calculated by conventional discrete control theory. However, the maximal sampling interval $\tau_{max} = \max_{x \in R^{4n}} \sigma(x)$ cannot be obtained without knowing σ . Thus, τ_{max} is set to be much larger than τ_{min} , $\tau_{max} > \tau_{min}$ in the algorithm to guarantee $\sigma(x) \leq \tau_{max}$.

3.2. The Selection of Feedback Gain for Controller

The system performance to some extent depends on the feedback gain. If the selected feedback gain is not proper for the control system, the τ_{min} in Theorem 1 may not exist, so that β -exponential stability and input-to-state stability cannot be satisfied even under the continuous control. Therefore, the feedback gain should be selected for satisfying the exponential stability and input-to-state stability in continuous control ($\sigma(x) = 0$) first. Otherwise, the cost function should be considered when we select the feedback gain. In dealing with nonlinear control problems, many optimal control theories are proposed, such as Hamilton–Jacobi–Bellman equations, Euler–Lagrange equations and Sontag’s formula [44,48]. However, it is difficult to apply those methods to solve this optimal control problem with the cost function described in Section 2. The reason is that solving the Hamilton–Jacobi–Bellman equations and Euler–Lagrange equations is extremely difficult. In addition, Sontag’s formula requires a fixed standard form of cost function, which does not coincide with our cost function. It is difficult to obtain the value of cost function directly. Therefore, instead of directly calculating the value of the cost function, inequalities for estimation are derived to select a proper feedback gain for guaranteeing the cost function within an upper bound.

Theorem 4. For given feedback gain K , γ , β , and $\tau_{min} = \min_{x \in R^N} \sigma(x)$ for global state space, which satisfies the condition of Proposition 1 and Assumption 1. Then the cost function (8) can be estimated by:

$$J < \frac{\lambda_{max}(Q)}{\beta^2 \lambda_{min}(P)} \{ \gamma n \eta T'_f \beta - [\gamma n \eta + V_0 \beta] (1 - e^{-\beta T'_f}) \} + \frac{\rho T'_f}{\tau_{min}}, \tag{19}$$

where,

$$T'_f = \frac{1}{\beta} \ln[(V_0 \beta - \gamma n \eta) / \nu] \geq T_f \tag{20}$$

Proof. From the proof of Theorem 1, the value of the Lyapunov function can be estimated by $V(t) \leq e^{-\beta t} V_0 + \gamma n \eta / \beta (1 - e^{-\beta t})$.

To integrate both sides of the above inequality during 0 and T_f , the cost of state can be estimated by: $\int_0^{T_f} x^T P x dt \leq \frac{1}{\beta^2} \{ \gamma n \eta T_f \beta - (\gamma n \eta + V_0 \beta) (1 - e^{-\beta T_f}) \}$.

The estimated terminal time T'_f for T_f can be obtained by solving the following inequality: $V(T_f) \leq e^{-\beta T_f} V_0 + \gamma n \eta / \beta (1 - e^{-\beta T_f}) = V_T$, and the time derivatives of V have the inequality $dV(T_f)/dt \leq (\gamma n \eta - V_0 \beta) e^{-\beta T_f}$.

Therefore, the result is: $T_f \leq \frac{1}{\beta} \ln[(V_0 \beta - \gamma n \eta) / v] = T'_f$.

The communication cost can be estimated by $c \leq \rho T'_f / \tau_{min} \leq \rho T_f / \tau_{min}$. Above all, the value of the cost function at terminal time T_f can be estimated by summing the estimation of state cost and communication cost. \square

For a given P for Lyapunov function, the decay rate β , and γ for the inhibition of disturbance effect, the minimal sampling interval τ_{min} and the feedback gain K can be figured out by conventional robust discrete control technique. Then, the upper bound of cost function J can be estimated by a given Lyapunov function value V_0 and V_T in initial time and terminal time by Theorem 4. The objective is to minimize the upper bound of J , so that the value of the cost function J can be guaranteed on a required level. Therefore, the feedback gain K , decay rate β , parameter γ for input-to-state stability, minimal sampling interval τ_{min} , and Lyapunov function parameter P , can be estimated by minimizing the upper bound of J . If we denote the right-hand side of inequality (19) by χ , it is:

$$\{K, \beta, P, \gamma\} = \arg \min_{\{K, \beta, P, \gamma\}} \chi(K, \beta, P, \gamma) \tag{21}$$

Some numerical optimization methods can be applied to solve this optimization problem. Let $\theta = \{K, \beta, P, \gamma\}$. The optimization process in one iteration can be depicted as follows:

1. For a given θ , τ_{min} is calculated by conventional discrete robust control technique;
2. The upper bound of cost function χ is obtained by Theorem 4, and R_k can be calculated;
3. Update θ by numerical optimization algorithms (such as GA optimization algorithm) with χ obtained in previous step;
4. Return to the first step until the stop criteria is satisfied.

The iteration stop condition depends on the value of χ and the iteration count and satisfies the design requirements. With the smallest upper bound of cost, the performance of control is guaranteed. The cost consists of state cost and communication cost. Thus, the Pareto Frontier curve may be calculated for generality. Then the optimal parameter θ can be easily obtained for any ρ .

3.3. Event-Triggered Control Algorithm

The self-triggered control is divided into two phrases. The first phrase is about parameter design, and the second phrase is online computing of triggering interval $\sigma(x(t_k))$. First, for a given power grid dynamic model (4) and Q , the τ_{min} is calculated. The best value of θ is designed by Theorem 4. Optimal searching algorithms consider both state and communication cost in cost function. If the feedback with gain K does not have a solution with given γ and β , β and γ should decrease and increase respectively until there is a solution of K . After θ , τ_{min} and τ_{max} are selected, the approximation error ϵ_1 , ϵ_2 and ϵ_3 are calculated. Meanwhile, the two-point Taylor expansion of Φ , ψ_1 and ψ_2 can be obtained by software such as Mathematica.

Second, the triggering interval is calculated online. The power system obtains new system state x_k from sensors, when a self-triggered time is up. Then, the time $t_{k+1} = t_k + \sigma(x(t_k))$ is calculated for the next triggering. For a system state x_k , the coefficient of polynomial respect to z is derived by $x^T H(z) x$. Then z_c is solved using Equation (18) by inverse iteration. Therefore, the triggering interval can be

obtained by z_c and (17). The new control output $u = -Kx(t_k)$ is calculated and applied to actuators. At last, the control output is updated at the next triggering time t_{k+1} .

4. Simulation Results

In this section, a simulation of power frequency control with distributed energy source demonstrates the effectiveness and advantages of our proposed control method. The subsystem frequencies are controlled by our proposed controller, which can save more costs under the consideration of communication and system state. Meanwhile, a comparison is carried out to verify the benefit on the control of power system. The simulation is performed in MATLAB 2010b.

We consider the electrical power network shown in Figure 4. Three subsystems are in the power system. It assumes that the composition of three electric power subsystems is same, which is illustrated in Figure 2. There are gas turbine generators, wind power generations and battery arrays in the system. Power supply is done to the electric power demand with these power generating machines. The gas turbine, wind power and battery power output are controllable.

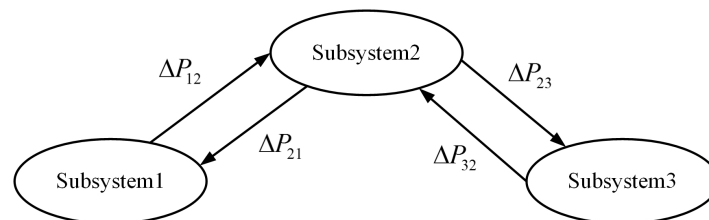


Figure 4. Power system structure for simulation

The parameters of each subsystem are given in Table 1.

Table 1. Parameter set.

Parameters (\$)	Symbols (Unit) (\$)	Values		
		Subsystem 1	Subsystem 2	Subsystem 3
Inertia constant	M (puMw s/Hz)	0.20	0.14	0.16
Damping constant	D (puMw/Hz)	0.26	0.26	0.23
Governor constant	T_g (s)	0.20	0.20	0.12
Gas turbine constant	T_d (s)	5.0	4.5	5.0
Regulation constant	R_g (Hz/pu Mw)	2.5	2.5	1.5
Synchronizing constant	T_{ij} (pu Mw)	0.50	0.5	0.5
TBC gain	K_i	0.1	0.08	0.1
Frequency bias	B_i (Mw/Hz)	0.1	0.1	0.08

The maximal norm of disturbance assumes to be 0.1, and the weight q for communication cost is set to 0.1. The contour map of cost upper bound with respect to exponential stability parameter β and input-to-state stability parameter γ is illustrated in Figure 5, and the relationship between β and τ_{min} is shown in Figure 6.

According to the cost upper bound contour map, if the parameter β is selected to be very low (lower than 0.02), then the effect of parameter γ is not significant. Meanwhile, it shows that the faster convergence rate (larger β) makes the physical cost (state cost) lower. However, according to the relationship between the τ_{min} and β illustrated in Figure 6, large β may bring a higher communication cost, because the controller has to reduce the triggering interval to satisfy higher physical cost requirements (faster rate of convergence). Thus, a tradeoff should be made to reduce the total cost. After solving the optimization problem described in (21) with MATLAB Optimization Toolbox, β and γ are obtained as 0.12 and 0.11, respectively. In addition, the feedback gain K and Lyapunov function parameter P are also calculated by the robust control design algorithm and LMI toolbox. The initial

state is set to 1, and the terminal time is calculated to be 10. The simulation is divided into two groups. The first group is the proposed algorithm with approximation method to calculate the triggering interval. The second method is the method proposed in [42], which is a widely used method in self-triggered control. We call it the “conventional method” in the following. The simulation results and comparisons are illustrated in Figures 7–11.

According to the simulation results in Figures 7–11, we know that the control method can make all states converge to zero with exponential rate β . Moreover, the curve with proposed control method converges slightly faster than the conventional method in the beginning, especially in the curve of Δf and Δx_g .

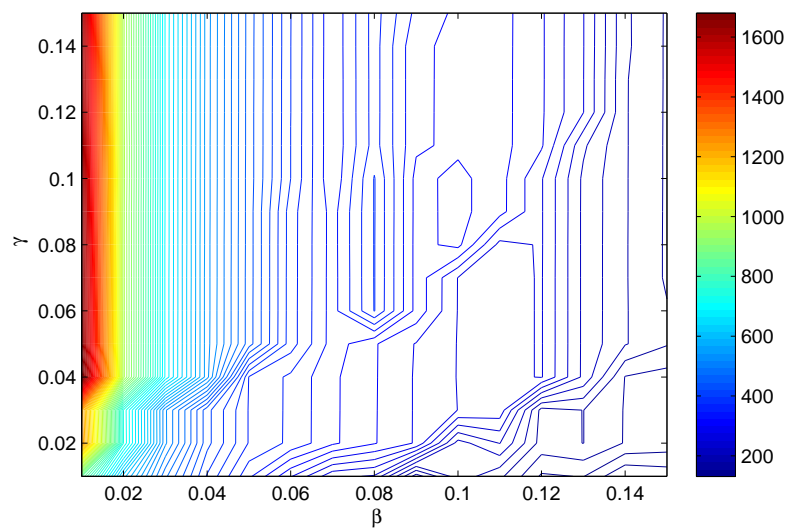


Figure 5. Contour map of cost upper bound with respect to β and γ .

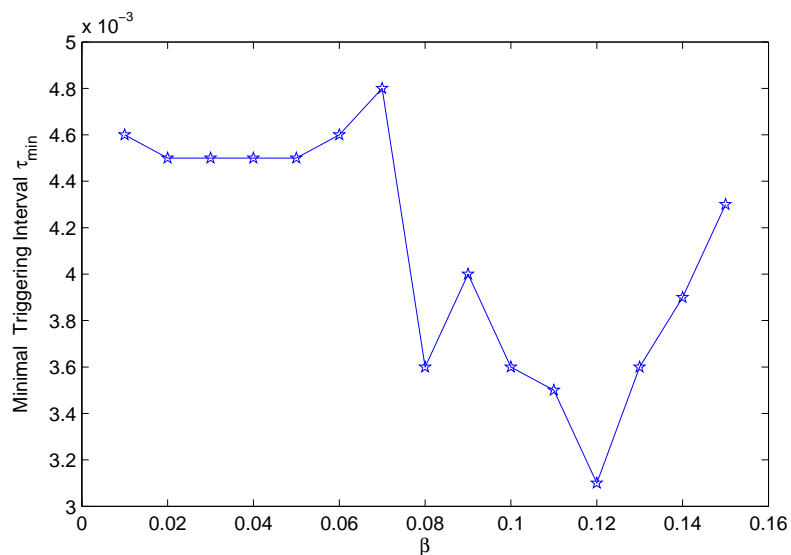


Figure 6. The minimal triggering interval curve with respect to β .

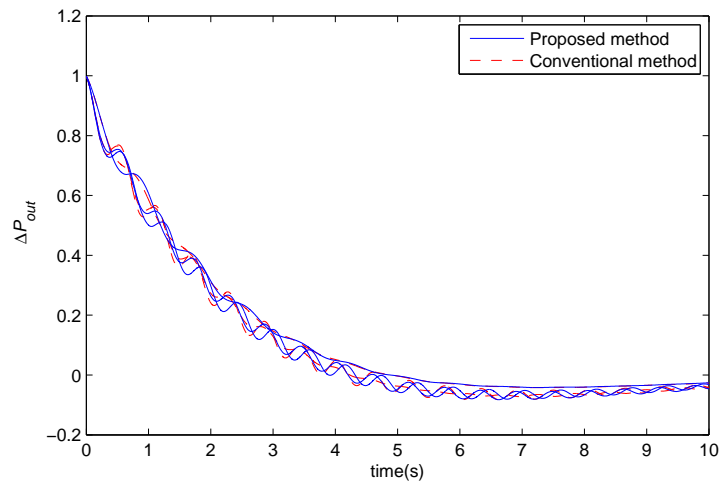


Figure 7. The output power deviation of each subsystem P_{out} .

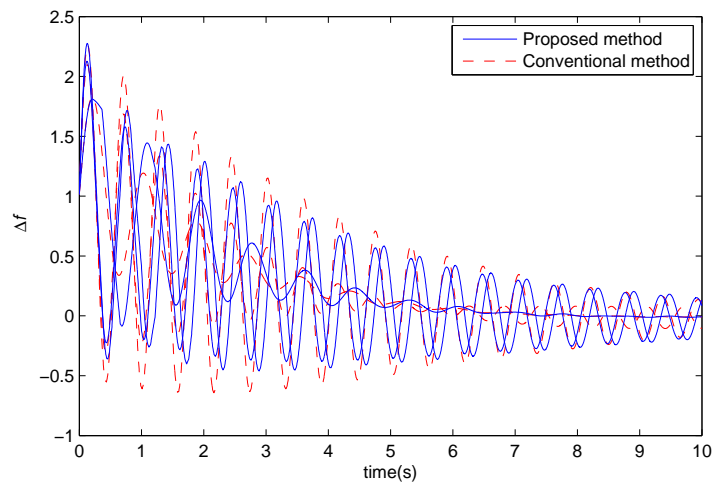


Figure 8. The frequency deviation Δf .

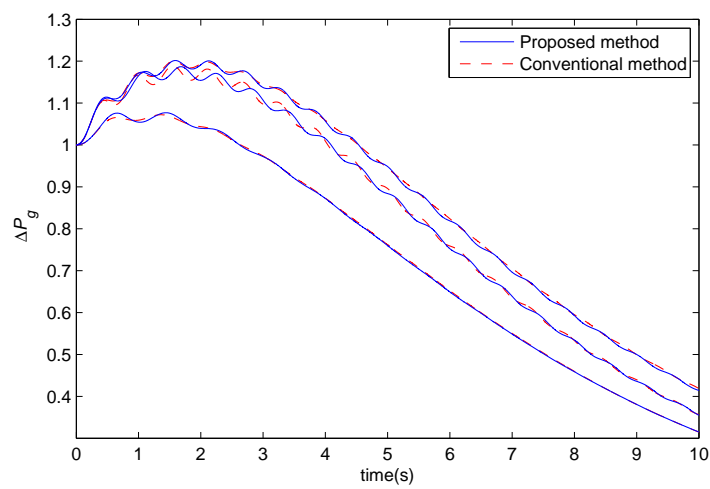


Figure 9. The power output deviation of the gas turbine generator P_g .

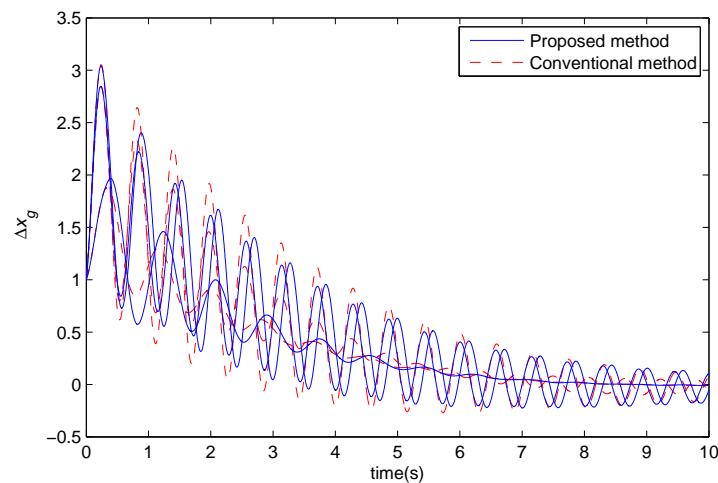


Figure 10. The governor input of the gas turbine generator Δx_g .

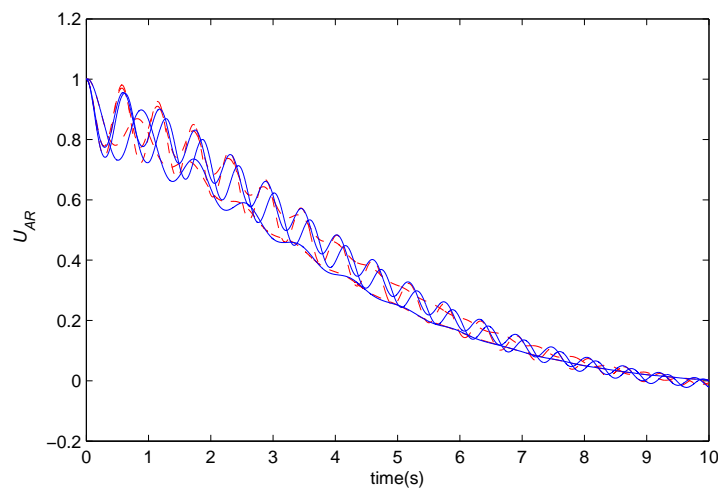


Figure 11. The regional demand U_{AR} .

At last, they are in the same magnitude. Above all, under the same exponential convergence rate β and input-to-state stability parameter γ requirement, the convergence rate or the physical cost seems almost same and satisfies the performance. The proposed method is effective in the frequency control application of power system. However, the communication should be considered in our proposed control algorithm. Therefore the comparison of communication cost is illustrated. As the sampling rate of classical control method is fixed, it causes the communication cost of the classical control method to be much higher than for the STC method [49,50]. We only compare the proposed STC method with the conventional STC method in Figure 12. The total cost is illustrated in Figure 13.

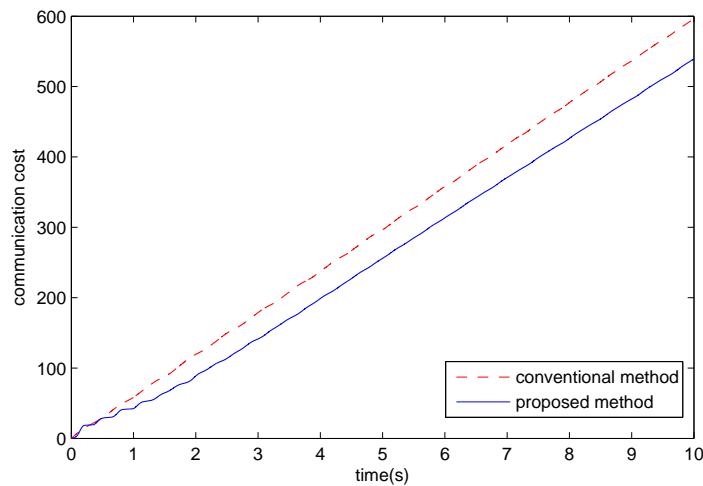


Figure 12. Communication cost comparison.

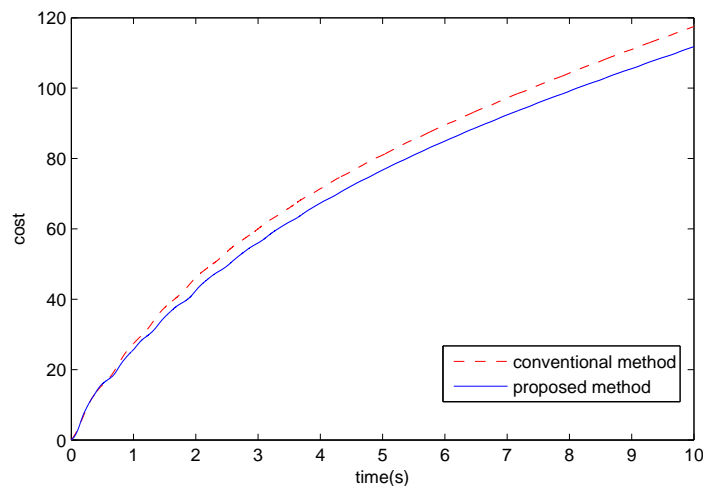


Figure 13. Cost curve comparison.

According to the communication cost comparison in Figure 12, it is known that the communication cost of the proposed self-triggered control method is lower than that of the conventional self-triggered control method. At the end of the simulation time, it costs about 530 control actions using the proposed self-triggered control method. In comparison, it costs about 600 control actions using conventional self-triggered control method. According to the definition of communication cost, the system takes 530 control actions for sensor data acquisition to compute control output with the proposed method, and needs 600 control actions using the conventional method. Based on the total cost curve comparison, the proposed self-triggered method costs less than the conventional method. At the end of simulation, the conventional method costs about 120 control actions, and the proposed method costs about 110 control actions. The cost of the proposed method is not much lower than for the conventional method. When the communication cost is high, bandwidth is limited, or communication network is publicly shared, the triggering time of proposed method further improves. Besides, the computation cost of calculating triggering time in the proposed method is reduced by the approximation method. Above all, the proposed method is better than the conventional method in frequency control application of power system, at least under this situation.

5. Conclusions

In this paper, a novel self-triggered control method is proposed and applied to the frequency control application of the power system. The power system dynamic model consists of multiple subsystems that have distributed energy sources. Physical cost and communication cost as two parameters of cost function are considered in the proposed model. On one hand, the equation for solving the triggering time is derived by the definition of exponential stability and the input of state stability, and an approximation algorithm is proposed to reduce computation costs. On the other hand, the upper bound of cost is derived. The feedback gain and parameters are selected, according to optimizing the upper bound of the cost. Thus, the system cost can be guaranteed under a required level. At last, a simulation of power system frequency control is carried out to demonstrate that the proposed method is effective and can save more costs than the conventional method. Compared with the distributed control scheme, the advantage of the centralized control scheme in STC is that it reduces the conservativeness of the control system, and further decreases the communication cost. Meanwhile, it may require more computational resources and time. Additionally, more communication networks are needed in the centralized control scheme. In future research, the application of self-triggered control method in the transient control of power system for avoiding cascade failure will be investigated.

Acknowledgments: This work was supported in part by the National Natural Science Foundation of China under Grant 61633005. This research is also funded by Chongqing Natural Science Foundation Grant cstc2016jcyjA0428 and Grant cstc2011jjA40013. This project was granted Fundamental Research Funds for the Central Universities cstc2016jcyjA0428.

Author Contributions: Zhiqin Zhu and Jian Sun conceived and designed the experiments; Zhiqin Zhu and Jian Sun performed the experiments; Jian Sun and Guanqiu Qi analyzed the data; Zhiqin Zhu contributed reagents/materials/analysis tools; Zhiqin Zhu and Jian Sun wrote the paper; Yi Chai and Yinong Chen provided technical support and revised the paper.

Conflicts of Interest: The authors declare no conflict of interest.

Appendix A. Proof of Theorem 1

For $t \in [t_k, t_{k+1}]$ and $t = t_k + \tau$, it is known that $x(t) = \zeta(\tau)x(t_k) + \xi(\tau)$, where,

$$\zeta(\tau) = I + \int_0^\tau e^{As} ds(A - BK), \xi(\tau) = \int_0^\tau e^{As} EW(s) ds$$

Therefore for the Lyapunov function

$$V(x(t)) = x(t)^T Px(t) = [\zeta(\tau)x(t_k) + \xi(\tau)]^T P[\zeta(\tau)x(t_k) + \xi(\tau)] \leq x(x_k)^T \zeta(\tau)^T P \zeta(\tau)x(x_k) + \xi^T P \xi.$$

We denote:

$$V'(x(t_k), \tau) = x(x_k)^T \zeta(\tau)^T P \zeta(\tau)x(x_k) + \xi^T P \xi.$$

We define ω as the mean of $EW(s)$ in the paper. For the given $\beta > 0$ and $\gamma > 0$, if,

$$\dot{V}' \leq -2\beta \dot{V}' + \gamma/2 \|W\|^2 + \gamma/2 \|\omega\|^2, \tag{A1}$$

where $\xi = \int_0^\tau e^{As} ds \omega$, then,

$$V'(x(t_k), \tau) \leq e^{-\beta\tau} V'(x(t_k), 0) + \int_0^\tau (\gamma/2 e^{-\beta s} \|W(s)\|^2 + \gamma/2 \|\omega\|^2) ds,$$

so that,

$$V(x(t)) \leq V'(x(t_k), \tau) \leq e^{-\beta\tau} V(x(t_k)) + \int_0^\tau \gamma/2e^{-\beta s} \|W(s)\|^2 ds + \int_0^\tau \gamma/2e^{-\beta s} \|\omega(s)\|^2 ds.$$

which means the dynamic system is of β -exponential stability. When $\|\omega\|^2 \leq n\eta$, we have $\|x\|^2 \leq n\gamma\eta/(\epsilon\beta)$ with initial state $x(t_k) = 0$. The inequality (A1) is:

$$d[x(t_k)^T \zeta(\tau)^T P \zeta(\tau) x(t_k)]/dt + 2\beta x(t_k)^T \zeta(\tau)^T P \zeta(\tau) x(t_k) \leq -d(\xi^T P \xi)/dt - 2\beta(\xi^T P \xi) + \gamma/2\|W\|^2 + \gamma/2\|\omega\|^2, \quad (A2)$$

and the inequality is:

$$\begin{aligned} -d(\xi^T P \xi)/dt - 2\beta(\xi^T P \xi) + \gamma/2\|W\|^2 &\geq \dot{\xi}^T P \xi - (2\beta + 1)(\xi^T P \xi) + \gamma/2\|W\|^2 \geq \\ &(\gamma/2 - r\epsilon e^{\alpha\tau})\|W\|^2 + [\gamma/2 - (2\beta + 1)(e^{\alpha\tau} - 1)r]\epsilon\|\omega\|^2. \end{aligned}$$

It should be noted that the left-hand side of inequality (A2) is equivalent to the left-hand side of inequality (9). If:

$$\begin{aligned} d[x(t_k)^T \zeta(\tau)^T P \zeta(\tau) x(t_k)]/dt + 2\beta x(t_k)^T \zeta(\tau)^T P \zeta(\tau) x(t_k) &\leq \\ (\gamma/2 - r\epsilon e^{\alpha\tau})\|W\|^2 + [\gamma/2 - (2\beta + 1)(e^{\alpha\tau} - 1)r]\epsilon\|\omega\|^2, \end{aligned}$$

then the inequality (A1) satisfies. When $\gamma/2 - r\epsilon e^{\alpha\tau} > 0$, and $\gamma/2 - (2\beta + 1)(e^{\alpha\tau} - 1)r > 0$, the above inequality holds if:

$$d[x(t_k)^T \zeta(\tau)^T P \zeta(\tau) x(t_k)]/dt + 2\beta x(t_k)^T \zeta(\tau)^T P \zeta(\tau) x(t_k) \leq 0.$$

When $\gamma/2 - r\epsilon e^{\alpha\tau} > 0$, and $\gamma/2 - (2\beta + 1)(e^{\alpha\tau} - 1)r \leq 0$, the above inequality holds if:

$$d[x(t_k)^T \zeta(\tau)^T P \zeta(\tau) x(t_k)]/dt + 2\beta x(t_k)^T \zeta(\tau)^T P \zeta(\tau) x(t_k) \leq [\gamma/2 - (2\beta + 1)(e^{\alpha\tau} - 1)r\epsilon]n\eta.$$

When $\gamma/2 - r\epsilon e^{\alpha\tau} \leq 0$, and $\gamma/2 - (2\beta + 1)(e^{\alpha\tau} - 1)r > 0$, the above inequality holds if:

$$d[x(t_k)^T \zeta(\tau)^T P \zeta(\tau) x(t_k)]/dt + 2\beta x(t_k)^T \zeta(\tau)^T P \zeta(\tau) x(t_k) \leq (\gamma/2 - r\epsilon e^{\alpha\tau})n\eta.$$

When $\gamma/2 - r\epsilon e^{\alpha\tau} \leq 0$, and $\gamma/2 - (2\beta + 1)(e^{\alpha\tau} - 1)r \leq 0$, the above inequality holds if:

$$\begin{aligned} d[x(t_k)^T \zeta(\tau)^T P \zeta(\tau) x(t_k)]/dt + 2\beta x(t_k)^T \zeta(\tau)^T P \zeta(\tau) x(t_k) &\leq \\ (\gamma/2 - r\epsilon e^{\alpha\tau})n\eta + [\gamma/2 - (2\beta + 1)(e^{\alpha\tau} - 1)r\epsilon]n\eta. \end{aligned}$$

Appendix B. Proof of Theorem 3

Since the approximation errors are given, under $\tau \in [\tau_{min}, \tau_{max}]$, we have $\Phi_{P,\beta}(\tau) - [H(z) + \epsilon I] \leq 0$. Hence,

$$x^T \Phi_{P,\beta}(\tau) x \leq x^T H(z) x + x^T \epsilon_1 I x. \quad (A3)$$

As we know, $|\psi_1(\tau) - h_1(z)| \leq \epsilon_2$ and $|\psi_2(\tau) - h_2(z)| \leq \epsilon_3$ where $\tau \in [\tau_{min}, \tau_{max}]$, thus if $x^T \Phi_{P,\beta}(\tau) x \leq x^T H(z) x + x^T \epsilon_1 I x \leq h_1(\tau) - \epsilon_2$ then $x^T \Phi_{P,\beta}(\tau) x \leq \psi_1(\tau) \leq \psi(\tau)$.

Therefore, the z_c calculated from Equation (18), makes the inequality (9) in Theorem 1.

References

1. Zhang, X.M.; Han, Q.L.; Yu, X. Survey on Recent Advances in Networked Control Systems. *IEEE Trans. Ind. Inform.* **2016**, *12*, 1740–1752.

2. Zhang, X.M.; Han, Q.L.; Zhang, B.L. An Overview and Deep Investigation on Sampled-Data-Based Event-Triggered Control and Filtering for Networked Systems. *IEEE Trans. Ind. Inform.* **2017**, *13*, 4–16.
3. Li, H.; Qiu, H.; Yu, Z.; Li, B. Multifocus image fusion via fixed window technique of multiscale images and non-local means filtering. *Signal Process.* **2017**, *138*, 71–85.
4. Li, H.; Liu, X.; Yu, Z.; Zhang, Y. Performance improvement scheme of multifocus image fusion derived by difference images. *Signal Process.* **2016**, *128*, 474–493.
5. Li, H.; Li, X.; Yu, Z.; Mao, C. Multifocus image fusion by combining with mixed-order structure tensors and multiscale neighborhood. *Inf. Sci.* **2016**, *349–350*, 25–49.
6. Sun, J.; Zheng, H.; Demarco, C.L.; Chai, Y. Energy Function-Based Model Predictive Control With UPFCs for Relieving Power System Dynamic Current Violation. *IEEE Trans. Smart Grid* **2016**, *7*, 2933–2942.
7. Anta, A.; Tabuada, P. To Sample or not to Sample: Self-Triggered Control for Nonlinear Systems. *IEEE Trans. Autom. Control* **2010**, *55*, 2030–2042.
8. Anta, A.; Tabuada, P. Exploiting Isochrony in Self-Triggered Control. *IEEE Trans. Autom. Control* **2012**, *57*, 950–962.
9. Miskowicz, M. *Event-Based Control and Signal Processing*; CRC Press: Boca Raton, FL, USA, 2015.
10. Zhu, Z.; Qi, G.; Chai, Y.; Li, P. A Geometric Dictionary Learning Based Approach for Fluorescence Spectroscopy Image Fusion. *Appl. Sci.* **2017**, *7*, 161.
11. Zhu, Z.; Qi, G.; Chai, Y.; Chen, Y. A Novel Multi-Focus Image Fusion Method Based on Stochastic Coordinate Coding and Local Density Peaks Clustering. *Future Internet* **2016**, *8*, 53.
12. Wang, K.; Qi, G.; Zhu, Z.; Chai, Y. A Novel Geometric Dictionary Construction Approach for Sparse Representation Based Image Fusion. *Entropy* **2017**, *19*, 306.
13. Sun, J.; Hu, Y.; Chai, Y.; Ling, R.; Zheng, H.; Wang, G.; Zhu, Z. L-infinity event-triggered networked control under time-varying communication delay with communication cost reduction. *J. Frankl. Inst.* **2015**, *352*, 4776–4800.
14. Sun, J.; Zheng, H.; Chai, Y.; Hu, Y.; Zhang, K.; Zhu, Z. A direct method for power system corrective control to relieve current violation in transient with UPFCs by barrier functions. *Int. J. Electr. Power Energy Syst.* **2016**, *78*, 626–636.
15. Velasco, M.; Fuertes, J.M.; Marti, P. The self triggered task model for real-time control systems. In Proceedings of the 24th IEEE Real-Time Systems Symposium, Cancun, Mexico, 3–5 December 2003; pp. 67–70.
16. Tsai, W.T.; Luo, J.; Qi, G.; Wu, W. Concurrent Test Algebra Execution with Combinatorial Testing. In Proceedings of the 2014 IEEE 8th International Symposium on Service Oriented System Engineering, Oxford, UK, 7–11 April 2014; pp. 35–46.
17. Wu, W.; Tsai, W.T.; Jin, C.; Qi, G.; Luo, J. Test-Algebra Execution in a Cloud Environment. In Proceedings of the 2014 IEEE 8th International Symposium on Service Oriented System Engineering, Oxford, UK, 7–11 April 2014; pp. 59–69.
18. Diaz-Cacho, M.; Delgado, E.; Barreiro, A.; Falcón, P. Basic Send-on-Delta Sampling for Signal Tracking-Error Reduction. *Sensors* **2017**, *17*, 312.
19. Zhu, Z.; Chai, Y.; Yin, H.; Li, Y.; Liu, Z. A novel dictionary learning approach for multi-modality medical image fusion. *Neurocomputing* **2016**, *214*, 471–482.
20. Rafael, S.; Sebastián, D.; Raquel, D.; Ernesto, F. Event-Based Control Strategy for Mobile Robots in Wireless Environments. *Sensors* **2015**, *15*, 30076–30092.
21. Tsai, W.T.; Qi, G. DICB: Dynamic Intelligent Customizable Benign Pricing Strategy for Cloud Computing. In Proceedings of the 2012 IEEE Fifth International Conference on Cloud Computing, Honolulu, HI, USA, 24–29 June 2012; pp. 654–661.
22. Tsai, W.T.; Qi, G.; Chen, Y. A Cost-Effective Intelligent Configuration Model in Cloud Computing. In Proceedings of the 2012 32nd International Conference on Distributed Computing Systems Workshops, Macau, China, 18–21 June 2012; pp. 400–408.
23. Tsai, W.T.; Qi, G.; Chen, Y. Choosing cost-effective configuration in cloud storage. In Proceedings of the 2013 IEEE Eleventh International Symposium on Autonomous Decentralized Systems (ISADS), Mexico City, Mexico, 6–8 March 2013; pp. 1–8.
24. Pandey, S.K.; Mohanty, S.R.; Kishor, N.; Catalão, J.P.S. Frequency regulation in hybrid power systems using particle swarm optimization and linear matrix inequalities based robust. *Int. J. Electr. Power Energy Syst.* **2014**, *63*, 887–900.

25. Bhatt, P.; Ghoshal, S.P.; Roy, R. Coordinated control of TCPS and SMES for frequency regulation of interconnected restructured power systems with dynamic participation from DFIG based wind farm. *Renew. Energy* **2012**, *40*, 40–50.
26. Mohanty, S.R.; Kishor, N.; Ray, P.K. Robust H-infinite loop shaping controller based on hybrid PSO and harmonic search for frequency regulation in hybrid distributed generation system. *Int. J. Electr. Power Energy Syst.* **2014**, *60*, 302–316.
27. Dai, Y.; Xu, Y.; Dong, Z.Y.; Wong, K.P.; Zhuang, L. Real-time prediction of event-driven load shedding for frequency stability enhancement of power systems. *IET Gen. Transm. Distrib.* **2012**, *6*, 914–921.
28. Cao, J.; Du, W.; Wang, H.; Chen, Z.; Li, H.F. A Novel Emergency Damping Control to Suppress Power System Inter-Area Oscillations. *IEEE Trans. Power Syst.* **2013**, *28*, 3165–3173.
29. Xu, Y.; Dong, Z.Y.; Luo, F.; Zhang, R.; Wong, K.P. Parallel-differential evolution approach for optimal event-driven load shedding against voltage collapse in power systems. *IET Gen. Transm. Distrib.* **2014**, *8*, 651–660.
30. Fiter, C.; Hetel, L.; Perruquetti, W.; Richard, J.-P. A state dependent sampling for linear state feedback. *Automatica* **2012**, *48*, 1860–1867.
31. Mazo, M.; Tabuada, P. Decentralized Event-Triggered Control Over Wireless Sensor/Actuator Networks. *IEEE Trans. Autom. Control* **2011**, *56*, 2456–2461.
32. Mazo, M., Jr.; Anta, A.; Tabuada, P. An ISS self-triggered implementation of linear controllers. *Automatica* **2010**, *46*, 1310–1314.
33. Heemels, W.P.M.H.; Donkers, M.C.F.; Teel, A.R. Periodic Event-Triggered Control for Linear Systems. *IEEE Trans. Autom. Control* **2013**, *58*, 847–861.
34. Namerikawa, T.; Kato, T. Distributed load frequency control of electrical power networks via iterative gradient methods. In Proceedings of the 50th IEEE Conference on Decision and Control and European Control (CDC-ECC), Orlando, FL, USA, 12–15 December 2011; pp. 7723–7728.
35. Keerqinhu, Qi, G.; Tsai, W.; Hong, Y.; Wang, W.; Hou, G.; Zhu, Z. Fault-Diagnosis for Reciprocating Compressors Using Big Data. In Proceedings of the Second IEEE International Conference on Big Data Computing Service and Applications (BigDataService), Oxford, UK, 29 March–1 April 2016; pp. 72–81.
36. Kundur, P. *Power System Stability and Control*; McGraw-Hill Education: New York, NY, USA, 1994.
37. Xiao, B.; Lam, H.K.; Li, H. Stabilization of Interval Type-2 Polynomial-Fuzzy-Model-Based Control Systems. *IEEE Trans. Fuzzy Syst.* **2017**, *15*, 205–217.
38. Tsai, W.T.; Qi, G.; Hu, K. Autonomous Decentralized Combinatorial Testing. In Proceedings of the 2015 IEEE Twelfth International Symposium on Autonomous Decentralized Systems, Taichung, Taiwan, 25–27 March 2015; pp. 40–47.
39. Tsai, W.T.; Qi, G. Integrated Adaptive Reasoning Testing Framework with Automated Fault Detection. In Proceedings of the 2015 IEEE Symposium on Service-Oriented System Engineering, San Francisco Bay, CA, USA, 30 March–3 April 2015; pp. 169–178.
40. Tsai, W.T.; Qi, G. Integrated fault detection and test algebra for combinatorial testing in TaaS (Testing-as-a-Service). *Simul. Model. Pract. Theory* **2016**, *68*, 108–124.
41. Zuo, Q.; Xie, M.; Qi, G.; Zhu, H. Tenant-based access control model for multi-tenancy and sub-tenancy architecture in Software-as-a-Service. *Front. Comput. Sci.* **2017**, *11*, 465–484.
42. Gommans, T.; Antunes, D.; Donkers, T.; Tabuada, P.; Heemels, M. Self-triggered linear quadratic control. *Automatica* **2014**, *50*, 1279–1287.
43. Guo, L.; Ljung, L. Exponential stability of general tracking algorithms. *IEEE Trans. Autom. Control* **1995**, *40*, 1376–1387.
44. Xiao, B.; Lam, H.K.; Song, G.; Li, H. Output-feedback tracking control for interval type-2 polynomial fuzzy-model-based control systems. *Neurocomputing* **2017**, *242*, 83–95.
45. Fiter, C.; Hetel, L.; Perruquetti, W.; Richard, J.-P. State dependent sampling: An LMI based mapping approach. In Proceedings of the 18th IFAC World Congress (IFAC'11), Milano, Italy, 28 August–2 September 2011.
46. Acikmese, B.; Carson, J.M.; Blackmore, L. Lossless Convexification of Nonconvex Control Bound and Pointing Constraints of the Soft Landing Optimal Control Problem. *IEEE Trans. Control Syst. Technol.* **2013**, *21*, 2104–2113.
47. Zhu, Z.; Qi, G.; Chai, Y.; Yin, H.; Sun, J. A Novel Visible-infrared Image Fusion Framework for Smart City. *Int. J. Simul. Process Model.* **2017**, in press.

48. Primbs, J.A.; Nevistic, V.; Doyle, J.C. Nonlinear Optimal Control: A Control Lyapunov Function and Receding Horizon Perspective. *Asian J. Control* **1999**, *1*, 14–24.
49. Tsai, W.; Qi, G.; Zhu, Z. Scalable SaaS Indexing Algorithms with Automated Redundancy and Recovery Management. *Int. J. Softw. Inform.* **2013**, *7*, 63–84.
50. Wang, S.; Zhang, P.; Fan, Y. Centralized event-triggered control of multi-agent systems with dynamic triggering mechanisms. In Proceedings of the 2015 27th Chinese Control and Decision Conference, Qingdao, China, 23–25 May 2015; pp. 2183–2187.



© 2017 by the authors. Licensee MDPI, Basel, Switzerland. This article is an open access article distributed under the terms and conditions of the Creative Commons Attribution (CC BY) license (<http://creativecommons.org/licenses/by/4.0/>).